AGU PUBLICATIONS

Geophysical Research Letters

RESEARCH LETTER
10.1002/2017GL072652

Key Points:
- The SMFe abundance in regolith minimally disturbed by the Chang'E-3 rocket exhaust was derived from in situ spectra and radiative transfer modeling
- The SMFe abundance indicates that the CE-3 landing site is submature
- The natural uppermost surficial regolith is more weathered than the regolith that was affected by rocket exhaust

Supporting Information:
- Supporting Information S1

Correspondence to:
Y. Wu,
wu@pmo.ac.cn

Citation:
Wang, Z., Y. Wu, D. T. Blewett, E. A. Cloutis, Y. Zheng, and J. Chen (2017), Submicroscopic metallic iron in lunar soils estimated from the in situ spectra of the Chang'E-3 mission, *Geophys. Res. Lett.*, *44*, 3485–3492, doi:10.1002/2017GL072652.

Received 19 JAN 2017
Accepted 2 APR 2017
Accepted article online 5 APR 2017
Published online 22 APR 2017

Submicroscopic metallic iron in lunar soils estimated from the in situ spectra of the Chang'E-3 mission

Zhenchao Wang[1], Yunzhao Wu[2], David T. Blewett[3], Edward A. Cloutis[4], Yongchun Zheng[5], and Jun Chen[1]

[1]Key Laboratory of Surficial Geochemistry, Ministry of Education, Department of Earth Sciences, Nanjing University, Nanjing, China, [2]Key Laboratory of Planetary Sciences, Purple Mountain Observatory, Chinese Academy of Sciences, Nanjing, China, [3]Planetary Exploration Group, The Johns Hopkins Applied Physics Laboratory, Laurel, Maryland, USA, [4]Department of Geography, University of Winnipeg, Winnipeg, Manitoba, Canada, [5]Key Laboratory of Lunar and Deep Space Exploration, National Astronomical Observatories of Chinese Academy of Sciences, Beijing, China

Abstract Submicroscopic metallic iron (SMFe) created by space weathering has strong effects on the optical properties of the lunar surface. Spectra measured in situ by the visible-near-infrared spectrometer (VNIS) on board the Chang'E-3 Yutu rover were used to investigate optical maturity differences at the CE-3 landing site caused by lander exhaust. SMFe abundances were estimated using Hapke's radiative transfer model. Analysis of the spectrum for a minimally disturbed soil indicates that it contains 0.368 wt % SMFe, corresponding to an I_s/FeO maturity index of ~53 and indicating that the landing site is submature. The soil at a location that was more disturbed contains 0.217 wt % SMFe, suggesting that the material removed by the rocket blast is more weathered than the regolith that remained behind. We conclude that maturity differences related to removal of the finest, highly mature particles play a major role in the observed reflectance changes associated with rocket blast.

Plain Language Summary Landed lunar missions can provide essential ground truth for calibration of orbital data as well as being able to investigate the lunar surface at high resolution. The Yutu rover aboard the Chang'E-3 lunar lander was used to investigate vertical and lateral variations in the optical and compositional properties of the lunar regolith. It was found that rocket exhaust from the landing disturbed the regolith to varying extents. Spectroscopic measurements and optical modeling showed that the abundance of submiscoscopic iron varied with distance from the landing site as well as vertically. The data suggest that space weathering is a rapid process relative to regolith turnover rates.

1. Introduction

Space weathering is the primary surface process on the Moon and other airless bodies, taking place continuously after they formed. This process reduces the albedo, decreases the strength of mineralogical absorption bands, and causes the spectral continuum to redden [e.g., *Fischer and Pieters*, 1994]. It has been long recognized that the primary mechanism causing these optical effects is the creation and accumulation of submicroscopic metallic iron (SMFe) [*Hapke*, 2001; *Lucey and Riner*, 2011; *Pieters et al.*, 1993, 2000; *Noble et al.*, 2001]. The SMFe is found throughout agglutinitic glass and on soil grains in vapor/sputter deposited and irradiated rims. The abundance of SMFe is clearly important in evaluating space weathering and hence the regolith evolution on the Moon. The effects of SMFe on the optical properties lunar soils have been well documented experimentally [*Allen et al.*, 1996; *Sasaki et al.*, 2003; *Noble et al.*, 2007; *Lucey and Noble*, 2008] and with physical modelling [*Hapke*, 2001; *Lucey and Riner*, 2011]. In early stages of study, it was noted that the SMFe changes the spectral features of lunar soils, reddening, darkening, and diminishing the spectral contrast of lunar soil spectra [e.g., *Fischer and Pieters*, 1994]. In the beginning of this century, a theoretic model of the optical effects of SMFe was built [*Hapke*, 2001]. Later, the variation of optical effects with SMFe particle size was recognized [*Noble et al.*, 2007; *Lucey and Riner*, 2011]. These workers documented that smaller SMFe (<~50 nm diameter) darkens and reddens spectra in the visible (Vis) wavelengths, with important but lesser effects in the near infrared (NIR). Larger SMFe (>~50 nm) lowers the albedo across the Vis/NIR range with little change in the overall shape of the continuum, although increasing abundance of smaller SMFe causes the edge of the red slope to move to progressively longer wavelengths.

The process producing SMFe, reduction of Fe^{2+} in lunar minerals or deposition of vapor produced by micrometeoroid impacts, mostly occurs at the very top surface (upper millimeter) [*Reedy et al.*, 1983; *Gault et al.*, 1974].

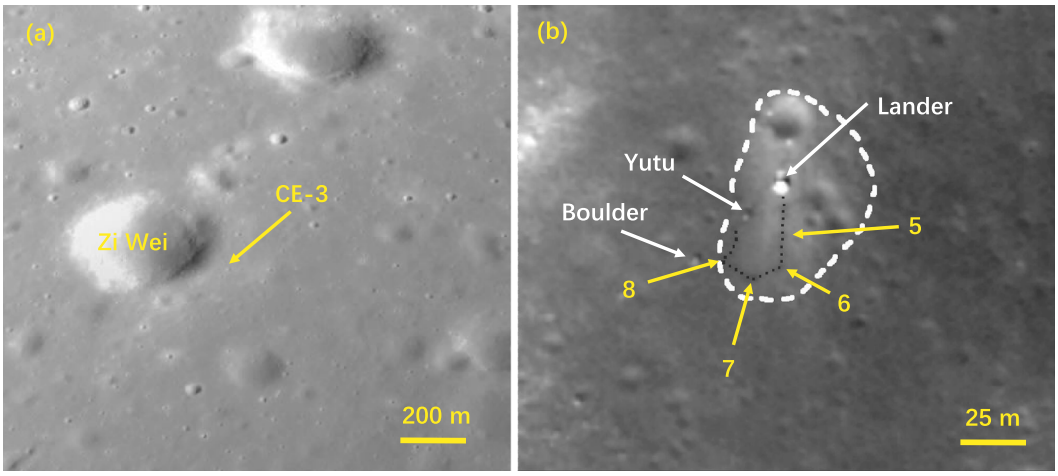

Figure 1. (a) Image taken by the CE-3 descent camera showing the location of the CE-3 landing site (44.1205°N, 19.5102°W). (b) LROC NAC image (M1147290066R) of CE-3 landing site. The locations of the four VNIS measurements (5 to 8) are shown. White dashed line outlines the blast zone; black dotted line highlights the rover tracks [*Clegg-Watkins et al.,* 2016].

The gardening, or turnover of the regolith by small impacts, mixes and buries mature soil; thus, units of mature soil exist to depths of at least a few meters [*Morris*, 1978]. Solar cosmic ray-produced radionuclides can be used to study gardening within the top ~1 cm of lunar cores. However, the very uppermost lunar dust layer has not been well sampled [*Noble et al*., 2011]. Hence, the optical properties of returned lunar samples may not be representative of the undisturbed lunar surface. It is important to estimate the SMFe content on the surface of the Moon using a technique that is sensitive to SMFe, such as reflectance spectrometry.

At 13:11:18 UTC on 14 December 2013, China's Chang'E-3 (CE-3) spacecraft landed on the Moon (Figure 1). The surface at the CE-3 landing site was disturbed by rocket exhaust from the spacecraft (e.g., brightened zone observed by the Lunar Reconnaissance Orbiter Camera (LROC) Narrow Angle Camera (NAC)) (Figure 1b) [*Clegg-Watkins et al*., 2016]. The visible-near-infrared spectrometer (VNIS) [*Liu et al*., 2013; *Liu et al*., 2014] on board the CE-3 Yutu rover collected in situ reflectance spectra within the disturbed area and at the edge. These spectra provide a unique opportunity to investigate the abundance of SMFe by characterizing regolith that was clearly disturbed to a greater extent by rocket exhaust as well as the minimally disturbed surface. In this paper, we use the in situ reflectance spectra acquired by VNIS to assess the SMFe content via Hapke's model [2001] for the spectral effects of SMFe. Refer to supporting information (SI) Text S1 for details of the VNIS instrument and operation.

2. Data

Chang'E-3 landed in northern Mare Imbrium at (44.1205°N, 19.5102°W, elevation = −2636.6 m) [*Wang et al*., 2014]. The landing site is ~50 m east of the rim of a 450 m crater, Zi Wei (Figure 1a). The landing site is within a unit belonging to the last major phase of lunar volcanism (Eratosthenian basalts) with an age of 1.98 Ga [*Morota et al*., 2010], ~2.35 Ga [*Wu et al*., 2015], or 2.96 Ga [*Hiesinger et al*., 2000]. These unsampled basalts are high FeO, middle to high TiO_2, and rich in olivine [*Staid et al*., 2011; *Wu et al*., 2016]. During the period that Yutu was mobile, four measurements (Sites 5–8) were made using the VNIS. Figure 1b shows the rover tracks and the locations of the four spectral measurements. Images from the LROC NAC taken after the landing revealed an area of increased reflectance interpreted as modification caused by rocket exhaust (Figure 1b) [*Clegg-Watkins et al*., 2016]. *Clegg-Watkins et al.* [2016] performed a study of the CE-3 landing site using LROC NAC images and found an increase in reflectance of ~10% within the blast zone relative to the background, similar to that at Apollo, Luna, and Surveyor landing sites. They reported changes in photometric behavior at the CE-3 site consistent with decreased backscattering and smoothing of the surface.

Of the four locations where VNIS spectra were collected, we consider Site 8 (~43 m from the lander) to be minimally disturbed soil (it is at the boundary of the diffuse blast zone defined by *Clegg-Watkins et al.* [2016] and is visually undisturbed) and Site 5 to represent soil that experienced the most disturbance. The

Table 1. Data Acquisition Conditions of the Two Sites Analyzed by VNIS and the M^3 Orbital Data (M3G20090207T061610)[a]

	M^3	Site 5	Site 8
Incidence angle (*i*°)	34.86	59.90	54.05
Emission angle (*e*°)	36.67	48.17	44.40
Phase (*g*°)	70.68	107.94	95.29
Local time	8:34	15:09	9:29
Location	44.032°N, 19.712°W	44.1148°N, 19.5153°W	

[a]Incidence and emission angles of the M3 spectrum have been corrected for the topography (see SI Text S3 for details).

in situ spectra of the regolith disturbed by rocket exhaust and the minimally disturbed uppermost regolith measured by the VNIS provide a unique opportunity for investigating the spectrum-altering effects of SMFe. In this study, we focus on Sites 5 and 8 because they represent the least and most disturbed end-members.

Ideally, we would assess the effects of SMFe by comparing spectra of soils with spectra of fresh rock of the same composition. However, VNIS did not obtain measurements for any freshly exposed rocks. Therefore, we selected a spectrum from the Chandrayaan-1 Moon Mineralogy Mapper (M^3) for a nearby, very fresh 350 m crater to represent unweathered rock. This location is ~4.7 km from the CE-3 site and is within the same stratigraphic unit as the CE-3 landing site. The crater materials are assumed to have an SMFe abundance of zero because this crater is very fresh and mass wasting on the crater walls will continuously expose unweathered material. It is possible that space weathering has caused a patina to develop to varying degrees on the rocks of the crater wall, in which case our assumption of zero SMFe content for the M^3 spectrum will lead to a slight underestimation of the SMFe content of the model spectra.

The M^3 Level 1 Optical Period 1B (OP1B) data, which have the highest spatial resolution (140 m/pixel) among all OPs M^3 global mode data and have been corrected for thermal emission [*Clark et al.*, 2011], were used for the analysis. Data acquisition conditions for the three spectra used in our analysis are shown in Table 1, and the spectra are plotted in Figure 2.

3. Method

We employed Hapke's treatment [2001] to model the abundance of SMFe of the landing site soil. Hapke's model calculates the bidirectional reflectance (*r*), while the measurement of VNIS used in this study is

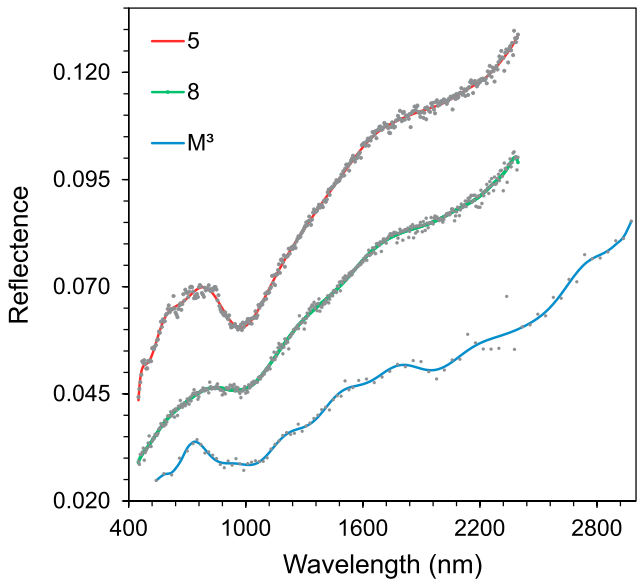

Figure 2. The original and smoothed VNIS and M^3 reflectance spectra. The dots are the original reflectance data, and the lines denote the spectrum after smoothing. Digital data are provided in Tables S1 and S2 (SI).

reflectance factor (REFF) (see SI Text S2 for definition). The REFF = $\pi r/\cos(i)$ and the combined Hapke's model is as follows:

$$\mathrm{REFF} = \frac{\omega_{\mathrm{ave}}}{4(\mu_0+\mu)}\{[1+B(g)]P(g)+H(\mu_0,\omega_{\mathrm{ave}})H(\mu,\omega_{\mathrm{ave}})-1\}, \tag{1}$$

where g is the phase angle, μ_0 is the cosine of the incidence angle (i), μ is the cosine of the viewing (emission) angle, and $B(g)$ is the backscatter function:

$$B(g) = \frac{B_0}{1+(1/h)\tan(g/2)}. \tag{2}$$

Here B_0 is the amplitude of the opposition effect (set to 1 in this case) [*Hapke*, 1981] and h is the angular width parameter of the opposition effect, approximated by

$$h = -\frac{3}{8}\ln(1-\varphi) \tag{3}$$

with the filling factor φ set to be 0.41 for lunar regolith [*Bowell et al.*, 1989]. $P(g)$ is the single-particle phase function. In this paper a second-order Legendre polynomial series is used:

$$P(g) = 1 + b\cos(g) + c\left(1.5\cos^2(g) - 0.5\right). \tag{4}$$

We assign $b = -0.4$ and $c = 0.25$ [*Mustard and Pieters*, 1989]. ω_{ave} is the average single-scattering albedo (SSA) of all the components in the medium, given by the following:

$$\omega_{\mathrm{ave}} = S_e + (1-S_e)\frac{(1-S_i)\Theta}{1-S_i\Theta}, \tag{5}$$

$$S_e = \frac{(n_h-1)^2 k_h^2}{(n_h+1)^2+k_h^2} + 0.05 \approx \frac{(n_h-1)^2}{(n_h+1)^2} + 0.05, \tag{6}$$

$$S_i = 1.014 - \frac{4}{n_h(n_h+1)^2}, \text{and} \tag{7}$$

$$\Theta = e^{-a_w D}. \tag{8}$$

Here S_e is the external surface scattering coefficient for Fresnel reflection from the surface of a particle averaged over all directions of incidence light on an external hemisphere of the particle. S_i is the internal surface scattering coefficient for light internally incident on the surface of the particle. n_h and k_h are the real and imaginary parts of the refractive index of the host. Θ is the internal-transmission factor representing the total fraction of light entering the particle that reaches another surface after one transit. α_ω is the absorption coefficient of an end-member component and can be calculated by its refractive index via $4\pi nk/\lambda$, where λ is the wavelength. $<D>$ is the mean path length of light in the particle, which is set to 30 μm in this work following *Hapke* [2012].

$H(\mu, \omega_{\mathrm{ave}})$ is the isotropic scattering function approximation [*Hapke*, 2012]:

$$H(\mu, w_{\mathrm{ave}}) = \left\{1 - \left(1-\sqrt{1-w_{\mathrm{ave}}}\right)\mu\left[r_0 + \left(1-\frac{r_0}{2}-r_0 u\right)\ln\frac{1+\mu}{\mu}\right]\right\}^{-1} \tag{9}$$

where

$$r_0 = \frac{2}{1+\sqrt{1-w_{\mathrm{ave}}}} - 1. \tag{10}$$

Hapke [2001] incorporated the spectral effects of space weathering into the calculation of absorption coefficients α of end-member components defined as below:

$$\alpha = \frac{4\pi n_h k_h}{\lambda} + \frac{36\pi z f \rho_h}{\lambda \rho_{Fe}} \tag{11}$$

where

$$z = \frac{n_h^3 n_{Fe} k_{Fe}}{\left(n_h^2 - k_{Fe}^2 + 2n_h^2\right)^2 + \left(2n_{Fe}k_{Fe}\right)^2}. \tag{12}$$

Here n and k are real and imaginary parts of the refractive index, respectively, and ρ is solid density. The three parameters refer to the host mineral and SMFe as indicated by the subscripts h and Fe, respectively. f represents the mass fraction of SMFe residing in the rim of a soil grain. These equations were used with the optical constants for metallic iron from *Paquin* 1995. The *Hapke*'s [2001] model accounts for the spectral effects of the smaller size range (<50 nm) of SMFe particles. To reduce the influence of spectral noise on the analysis, both the in situ and M^3 spectra were smoothed by B-spline fitting, which is a spline function that has been demonstrated to be useful for M^3 spectral smoothing [*Zhang et al*., 2016].

The spectrum of the visually undisturbed soil, Site 8, was used as the base. The modeled spectra for M^3 and Site 5 were created by adding various amounts of SMFe in increments of 0.001 wt % and then comparing to the spectrum of Site 8 by matching spectral shapes through the Spectral Angle (SA) parameter [*Kruse et al*., 1993]. The SA parameter is a measure of the similarity of two spectra, determined as the angle between the spectra in n-dimensional space, where n is the number of spectral channels. We chose the SA rather than other spectral matching methods because it is insensitive to effects of absolute reflectance related to the illumination geometry and instrument calibration. The comparison was performed over the wavelength range 0.68–2.20 μm, in order to avoid the effects of thermal emission from the lunar surface at longer wavelengths (>2.20 μm) and low SNR at shorter wavelengths (<0.68 μm) [*He et al*., 2014]. The optimal fit for the mass fraction of SMFe was determined by minimizing the SA between the target spectrum and the modeled spectrum.

Our modeling is done with the *Hapke* [2001] treatment, which handles the smaller (<50 nm) SMFe particles, responsible for both darkening and reddening. Particles >~50 nm mainly induce darkening [*Noble et al*., 2007; *Lucey and Noble*, 2008; *Lucey and Riner*, 2011]. The mostly flat slope of the spectrum of larger SMFe particles that are actually present in a soil would tend to lessen the slope when in a mixture with the smaller SMFe. Therefore, it is likely that our best fit spectral models somewhat underestimate the abundance of small SMFe relative to the actual soil content. Moreover, little patina existing on the surface of the rock but we assume that its SMFe to be zero will also cause an underestimation.

4. Results and Discussion

The reflectance spectra for Sites 5 and 8 and the M^3 fresh crater are shown in Figure 2. Compared with Site 8, Site 5 has ~60% greater reflectance between 450–760 nm and ~63% greater absorption strength at ~1000 nm but a similar visible- and near-infrared continuum slope (38 nm^{-1}, with a linear continuum fit at ~750 and ~1500 nm). These characteristics indicate that the disturbed regolith (Site 5) is less mature than the minimally disturbed soil (Site 8). We suggest that the lander's rocket exhaust blew away the fine, uppermost mature particles leaving less mature materials at the surface. This process strongly affected Site 5 but was much less prevalent at Site 8 which is farthest away from the landing site and is on the outer edge of the disturbed area as mapped by *Clegg-Watkins et al.* [2016] (Figure 1). The M^3 spectrum has a less steep continuum and a deeper 1000 nm mafic mineral absorption than the Site 5 spectrum, which is consistent with the fact that the M^3 spectrum is from a fresh crater. The absolute reflectance of the M^3 spectrum is lower than that of the in situ reflectance, probably related to calibration differences between the data sets. For example, previous comparisons found that the M^3 OP1B data have lower reflectance than Optical Period 2 (OP2C1) data [*Besse et al*., 2013; *Wu et al*., 2016]. Note that the SMFe determination in this paper is focused on the spectral shape via the Spectral Angle parameter, not the absolute value of reflectance.

Figure 3 shows the measured and modeled reflectance with the optimal model for both Site 5 and M^3. For ease of comparison, the reflectance has been normalized to unity at 1000 nm in Figure 3b. The model reproduces well for both M^3 and Site 5. The best SA match for the Site 8 spectrum was found to be the M^3 spectrum plus an SMFe abundance of 0.368 wt %. The best SA match between Site 8 and Site 5 was found for the Site 5

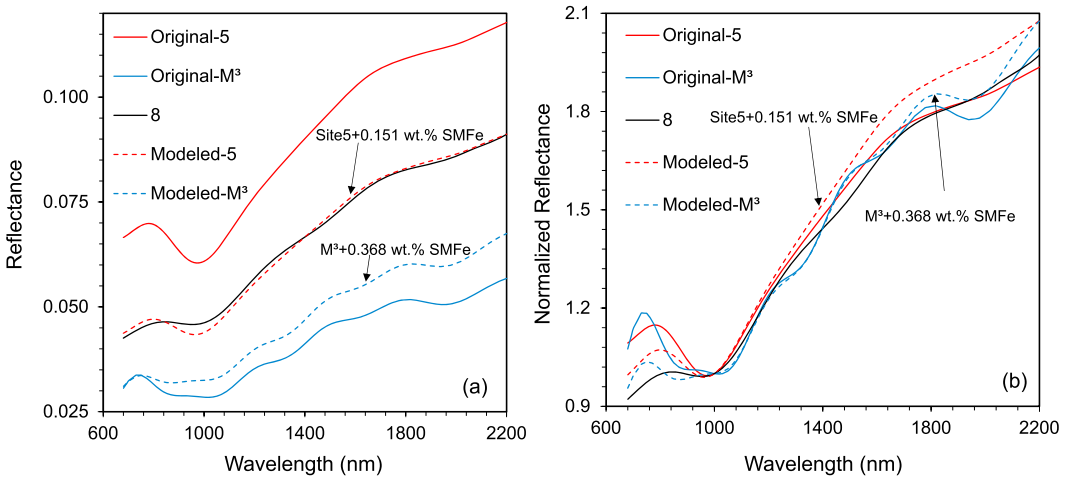

Figure 3. (a) Original and (b) normalized spectra of the optimal modeling results.

spectrum plus an SMFe abundance of 0.151 wt %. Hence, the SMFe abundance of the visually undisturbed soil, Site 8, is 0.368 wt % and that of the most-disturbed soil, Site 5, is 0.217 wt %. (Refer to the SI Figure S1 for examples of model spectra with lesser and greater SMFe abundances than in the optimal case.) This analysis suggests that the maturity difference between Site 5 and Site 8 is a result of greater SMFe abundance in Site 8. Considering that the disturbance depth of Site 5 is very shallow and only the finest fraction of the regolith was affected, this finding reveals that the uppermost surface is much more weathered than material immediately below the surface. Hence, our spectral findings are consistent with those from the photometric analysis of *Clegg-Watkins et al.* [2016], who concluded that the CE-3 site underwent a "change in surface maturity by removal of highly mature very fine-grained regolith components." In returned lunar samples, it is found that the finer fractions of the regolith are the most mature (have the highest I_s/FeO) (see discussion in *Lucey et al.* [2006]).

It is well known that disturbance of the lunar surface by astronauts and rovers leads to changes in albedo [e.g., *Kaydash et al.*, 2011; *Clegg et al.*, 2014]. These changes are mainly attributed to modification of the porosity and roughness of the surface; control on albedo by porosity is also predicted from theory [*Hapke*, 2008]. Thus, it is reasonable to ask whether such disturbance could lead to differential changes in albedo, that is, color changes, which might include differences in spectral slope or absorption band strength. *Ohtake et al.* [2010] presented laboratory spectra for lunar sample 62231 measured for three different porosities. In agreement with *Hapke* [2008], they found that the reflectance increased with decreasing porosity. *Ohtake et al.* [2010] also found that the spectral slope decreased slightly with decreasing porosity, although they found no change in 1000 nm band depth or in the center wavelength of the absorption. The VNIS spectra clearly show a stronger absorption band in the disturbed location (Site 5) than in the minimally disturbed location (Site 8). Therefore, the spectral differences caused by descent engine exhaust that we are examining are not likely to be related to a change in porosity.

Morris [1980] describes the relationship between the abundance of SMFe, the FeO content, and the soil maturity index I_s/FeO. Using equation (4) of *Morris* [1980], we can compute the I_s/FeO of the undisturbed CE-3 landing site using our determined SMFe content (0.368 wt %) and the soil FeO abundance derived from the Yutu rover's Active Particle-induced X-ray Spectrometer, which is 21.5 wt % [*Neal et al.*, 2015]. The calculated I_s/FeO value for Site 8 is 53, which falls in the "submature" range (30–60) [*Morris*, 1980]. Here it should be noted that the SMFe abundance that we estimate from the *Hapke* [2001] spectral model corresponds to particles $<$~50 nm in diameter. The ferromagnetic resonance technique used by *Morris* [1980] to determine the I_s values is sensitive to iron particles in the diameter range ~4–33 nm. Thus, our spectral estimates of the abundance of SMFe include the influence of particles in the ~33–50 nm range that are not sensed by magnetic resonance. As a result, using our spectrally determined SMFe abundance in *Morris's* [1980] equation will tend to slightly overestimate the I_s/FeO value. However, as discussed at the end of section 3, our spectral estimate of SMFe content is likely to be slightly too low because of the type of parameter used to determine the best fit. This underestimation of SMFe content is balanced to some degree by the tendency to

overestimate I_s in Morris's equation caused by the difference in SMFe particle sizes sensed by optical spectroscopy and ferromagnetic resonance.

If we assume that the soil at mare craters began to accumulate SMFe at a steady rate immediately after the craters formed, then the I_s/FeO value can be taken as an approximate indicator of age. For comparison, I_s/FeO is 29 for soil returned from Steno Crater at Apollo 17 [*Morris*, 1978] and 57 for Surveyor crater at Apollo 12 [*Meyer*, 2011]. The I_s/FeO that we found for the CE-3 landing site is ~53, so the age of Zi Wei crater at the landing site may be intermediate between that of Steno crater and Surveyor crater. The age of Steno Crater is 110 Ma [*Arvidson et al*., 1976] and the age of Surveyor crater is 240 Ma [*Funkhouser*, 1971], as determined by radioisotope dating of returned samples. The age of Zi Wei crater has been estimated as 27–80 Ma using crater size-frequency distribution measurements [*Xiao et al*., 2015] and ~100 Ma using the morphologic classification [*Basilevsky et al*., 2015]. Our result is broadly consistent with previous research and indicates the CE-3 landing site is relatively young.

5. Conclusions

The CE-3 Yutu rover measured in situ spectra of soils disturbed to different degrees, offering a unique opportunity for investigation of space weathering. We estimate the SMFe abundance of the least disturbed location at the landing site to be 0.368 wt %. This SMFe abundance, when combined with the site's measured FeO content, yields a soil maturity index (I_s/FeO) value of ~53, indicating that the undisturbed soils of the landing site are submature.

We find that the soil exposed by the CE-3 lander exhaust (Site 5) has substantially lower SMFe content than the minimally disturbed area (Site 8): 0.217 wt % at Site 5 versus 0.368 wt % at Site 8. The disturbance likely involves only the very uppermost accumulation of the finest dust. Therefore, the reflectance changes associated with rocket blast at spacecraft landing sites can primarily be attributed to maturity differences related to removal of fine, highly mature particles.

Acknowledgments

We thank the entire Chang'E-3 team for making the mission a success and providing the data. CE-3 data are archived at the website of the National Astronomical Observatories, Chinese Academy of Sciences: http://moon.bao.ac.cn/ceweb/datasrv/dmsce1.jsp. This research was supported by the National High Technology Research and Development Program of China (863 Program: 2015AA123704), the National Natural Science Foundation of China (41422110 and 41490633), the Science and Technology Development Fund of Macau (020/2014/A1), and Minor Planet Foundation of Purple Mountain Observatory. The contribution of D.T.B. was made possible by the Chinese Academy of Sciences President's International Fellowship Initiative, grant 2015VEB057 and by NASA Lunar Data Analysis Program grant NNX16AN55G. E.A.C. thanks NSERC and the Canadian Space Agency for supporting this study. We would like to thank Paul Lucey and an anonymous reviewer for helpful suggestions, which led us to substantially improve this paper.

References

Allen, C. C., R. V. Morris, and D. S. McKay (1996), An experimental analog to maturing lunar soil, *Proc. Lunar Planet. Sci. Conf., 27th,* 13–14.

Arvidson, R., R. Drozd, E. Guinness, C. Hohenberg, C. Morgan, and R. Morrison (1976), Cosmic ray exposure ages of Apollo 17 samples and the age of Tycho, *Proc. Lunar Planet. Sci. Conf., 7th*, 2817–2832.

Basilevsky, A. T., A. M. Abdrakhimov, J. W. Head, C. M. Pieters, Y. Wu, and L. Xiao (2015), Geologic characteristics of the Luna 17/Lunokhod 1 and Chang'E-3/Yutu landing sites, northwest Mare Imbrium of the Moon, *Planet. Space Sci.*, *117*, 385–400.

Besse, S., J. Sunshine, M. Staid, J. Boardman, C. Pieters, P. Guasqui, E. Malaret, S. McLaughlin, Y. Yokota, and J.-Y. Li (2013), A visible and near-infrared photometric correction for Moon Mineralogy Mapper (M^3), *Icarus*, *222*, 229–242.

Bowell, E., B. Hapke, D. Domingue, K. Lumme, J. Peltoniemi, and A. W. Harris (1989), Applications of photometric models to asteroids, in *Asteroids II*, edited by R. Binzel, T. Gehrels, and M. Matthews, pp. 524–556, Univ. of Ariz. Press, Tucson.

Clark, R. N., C. M. Pieters, R. O. Green, J. W. Boardman, N. E. Petro (2011), Thermal removal from near-infrared imaging spectroscopy data of the Moon, *J. Geophys. Res., 116*, E00G16, doi:10.1029/2010JE003751.

Clegg, R. N., B. L. Jolliff, M. S. Robinson, B. W. Hapke, and J. B. Plescia (2014), Effects of rocket exhaust on lunar soil reflectance properties, *Icarus*, *227*, 176–194.

Clegg-Watkins, R. N., B. L. Jolliffa, A. Boydc, M. S. Robinsonc, R. Wagnerc, J. D. Stoparc, J. B. Plesciad, and E. J. Speyerer (2016), Photometric characterization of the Chang'e-3 landing site using LROC NAC images, *Icarus*, *273*, 84–95.

Fischer, E. M., and C. M. Pieters (1994), Remote determination of exposure degree and iron concentration of lunar soils using VIS-NIR spectroscopic methods, *Icarus*, *111*, 475–488.

Funkhouser, J. (1971), Noble gas analysis of KREEP fragments in lunar soils 12033 and 12070, *Earth Planet. Sci. Lett.*, *12*, 263–272.

Gault, D. E., F. Hoerz, D. E. Brownlee, and J. B. Hartung (1974), Mixing of the lunar regolith, *Proc. Lunar Sci. Conf., 5th*, 2365–2386.

Hapke, B. (1981), Bidirectional reflectance spectroscopy: 1. Theory, *J. Geophys. Res.*, *86*, 3039–3054.

Hapke, B. (2001), Space weathering from Mercury to the asteroid belt, *J. Geophys. Res.*, *106*, 10,039–10,073.

Hapke, B. (2008), Bidirectional reflectance spectroscopy. 6. Effects of porosity, *Icarus*, *195*, 918–926.

Hapke, B. (2012) *Theory of Reflectance and Emittance Spectroscopy*, 2nd ed., Cambridge Univ. Press, Cambridge, U. K.

He, Z. P., et al. (2014), Operating principles and detection characteristics of Visible and Near-Infrared Imaging Spectrometer (VNIS) in Chang'E-3 project, *Res. Astron. Astrophys.*, *14*, 1567–1577.

Hiesinger, H., R. Jaumann, G. Neukum, and J. W. Head III (2000), Age of mare basalts on the lunar nearside, *J. Geophys. Res.*, *105*(E12), 29,239–29,275, doi:10.1029/2000JE001244.

Kaydash, V., Y. Shkuratov, V. Korokhin, and G. Videen (2011), Photometric anomalies in the Apollo landing sites as seen from the lunar Reconnaissance Orbiter, *Icarus*, *211*, 89–96.

Kruse, F. A., A. B. Lefkoff, J. W. Boardman, K. B. Heidebrecht, A. T. Shapiro, P. J. Barloon, and A. F. H. Goetz (1993), The spectral image processing system (SIPS)—Interactive visualization and analysis of imaging spectrometer data, *Remote Sens. Environ.*, *44*, 145–163.

Liu, B., J.-Z. Liu, G.-L. Zhang, Z.-C. Ling, J. Zhang, Z.-P. He, B.-Y. Yang, and Y.-L. Zou (2013), Reflectance conversion methods for the VIS/NIR imaging spectrometer aboard the Chang'E-3 lunar rover: Based on ground validation experiment data, *Res. Astron. Astrophys.*, *13*(7), 862–874.

Liu, B., C.-L. Li, G.-L. Zhang, R. Xu, J.-J. Liu, X. Ren, X. Tan, X.-X. Zhang, W. Zuo, and W.-B. Wen (2014), Data processing and preliminary results of the Chang'E-3 VIS/NIR imaging spectrometer in-situ analysis, *Res. Astron. Astrophys.*, *14*, 1578–1594.

Lucey, P. G., and S. K. Noble (2008), Experimental test of a radiative transfer model of the optical effects of space weathering, *Icarus*, *197*, 348–353, doi:10.1016/j.icarus.2008.05.008.

Lucey, P. G., and M. A. Riner (2011), The optical effects of small iron particles that darken but do not redden: Evidence of intense space weathering on Mercury, *Icarus*, *212*, 451–462, doi:10.1016/j.icarus.2011.01.022.

Lucey, P. G., et al. (2006), Understanding the lunar surface and space-Moon interactions, in *New Views of the Moon, Rev. Mineral. Geochem.*, vol. 60, edited by B. L. Jolliff et al., pp. 84–219.

Meyer, C. (2011), Lunar sample compendium, *Proc. Lunar Planet. Sci. Conf., 42nd*, Abstract 1533.

Morota, T., et al. (2010), Timing and characteristics of the latest mare eruption on the Moon, *Earth Planet. Sci. Lett.*, *302*, 255–266, doi:10.1016/j.epsl.2010.12.028.

Morris, R. V. (1978), The surface exposure (maturity) of lunar soils; some concepts and is/FeO compilation, *Proc. Lunar Planet. Sci. Conf., 9th,* 2287–2297.

Morris, R. V. (1980), Origins and size distribution of metallic iron particles in the lunar regolith, *Proc. Lunar Planet. Sci. Conf., 11st*, 1697–1712.

Mustard, J., and C. Pieters (1989), Photometric phase functions of common geologic minerals and applications to quantitative analysis of mineral mixture reflectance spectra, *J. Geophys. Res.*, *94*(13), 619–634.

Neal, C. R., et al. (2015), Regolith at the Chhang'E-3 landing site: A new type of mare basalt composition, *Proc. Lunar Planet. Sci. Conf., 46th,* Abstract 1641.

Noble, S. K., C. M. Pieters, L. A. Taylor, R. V. Morris, C. C. Allen, D. S. McKay, and L. P. Keller (2001), The optical properties of the finest fraction of lunar soil: Implications for space weathering, *Meteorit. Planet. Sci.*, *36*, 31–42, doi:10.1111/j.1945-5100.2001.tb01808.x.

Noble, S. K., C. M. Pieters, and L. P. Keller (2007), An experimental approach to understanding the optical effects of space weathering, *Icarus*, *192*, 629–642.

Noble, S. K., L. P. Keller, and C. Christoffersen (2011), Sampling the uppermost surface of airless bodies, *Solar System Sample Return Mission Conf.*, Abstract 5008.

Ohtake, M., et al. (2010), Deriving the absolute reflectance of lunar surface using SELENE (Kaguya) multiband imager data, *Space Sci. Rev.*, *154*, 57–77.

Paquin, R. A. (1995), Properties of metals, in *Handbook of Optics Volume II: Devices, Measurements, and Properties*, edited by M. Bass et al., pp. 35.31–35.78 , McGraw-Hill, New York.

Pieters, C. M., E. M. Fischer, O. Rode, and A. Basu (1993), Optical effects of space weathering: The role of the finest fraction, *J. Geophys. Res.*, *98*, 20,817–20,824, doi:10.1029/93JE02467.

Pieters, C. M., L. A. Taylor, S. K. Noble, L. P. Keller, B. Hapke, R. V. Morris, C. C. Allen, D. S. McKay, and S. Wentworth (2000), Space weathering on airless bodies: Resolving a mystery with lunar samples, *Meteorit. Planet. Sci.*, *35*, 1101–1107, doi:10.1111/j.1945-5100.2000.tb01496.x.

Reedy, R. C., J. R. Arnold, and D. Lal (1983), Cosmic-ray record in solar system matter, *Science*, *219*, 127–135.

Sasaki, S., E. Kurahashi, C. Yamanaka, and K. Nakamura (2003), Laboratory simulation of space weathering: Changes of optical properties and TEM/ESR confirmation of nanophase metallic iron, *Adv. Space Res.*, *31*, 2537–2542.

Staid, M. I., et al. (2011), The mineralogy of late stage lunar volcanism as observed by the Moon Mineralogy Mapper on Chandrayaan-1, *J. Geophys. Res., 116*, E00G10, doi:10.1029/2010JE003735

Wang, F. F., et al. (2014), A new lunar absolute control point: Established by images from the landing camera on Chang'e-3, *Res. Astron. Astrophys.*, *14*, 1543–1556.

Wu, Y. Z., J. W. Head, C. M. Pieters, A. T. Basilevsky, and L. Li (2015), Regional geology of the Chang'E-3 landing zone II, *Proc. Lunar Planet. Sci. Conf., 46th*, Abstract 2187.

Wu, Y. Z., et al. (2016), Seamless hyperspectral high spatial mosaic derived from Chang'E-1 IIM, *Proc. Lunar Planet. Sci. Conf., 47th*, Abstract 1405.

Xiao, L., et al. (2015), A young multilayered terrane of the northern Mare Imbrium revealed by Chang'E-3 mission, *Science*, *347*, 1226–1229.

Zhang, X., Y. Wu, Z. Ouyang, R. Bugiolacchi, Y. Chen, X. Zhang, W. Cai, A. Xu, and Z. Tang (2016), Mineralogical variation of the late stage mare basalts, *J. Geophys. Res. Planets*, *121*, 2063–2080, doi:10.1002/2016JE005051.